Modelling of the Preheating Section in Anode Baking Furnaces - A CFD Approach and a Mass-Energy Conservation Method

Behrad Asgari[1] and Louis Gosselin[2]
1. Postdoctoral Fellow
2. Full Professor
Aluminium Research Centre – REGAL & Department of Mechanical and Industrial Engineering, Université Laval, Québec, Canada
Corresponding author: louis.gosselin@gmc.ulaval.ca
https://doi.org/10.71659/icsoba2025-el011

Abstract

Among the various stages in anode production, the baking process stands out as the most energy-intensive, cost-demanding, and quality-defining phase. Despite its significance, one critical section of the process, i.e., the preheating section, remains challenging to analyse, primarily due to its inherent complexities, such as the release of volatiles from the anodes and their subsequent combustion in the flue channel. This knowledge gap has persisted for decades, largely due to the lack of advanced modelling approaches tailored to the unique challenges of the preheating section. In this study, we introduce a Computational Fluid Dynamics (CFD) model of the preheating section in anode baking furnaces. This model provides insight into the intricate interactions of volatile release, heat transfer, and combustion phenomena. Complementing this, we introduce a simplified model based on mass and energy conservation principles, and accounting for the effects of tie-bricks within the flue channel, a critical aspect often overlooked by previous studies. Our findings reveal a good accuracy of the proposed models, with an average temperature prediction discrepancy of 5 °C between the CFD and the simplified model based on mass-energy conservation. Moreover, while the CFD simulation requires approximately three hours of computational time per furnace section, the simplified model achieves equivalent precision in just three seconds, offering an unprecedented combination of speed and reliability.

Keywords: Anode baking furnace, Preheating section, CFD simulation, Mass-energy conservation, Volatile release and combustion.

1. Introduction

Aluminium, valued for its low density, high strength-to-weight ratio, and excellent corrosion resistance, is vital across many industries [1]. Its production begins with bauxite, refined into alumina through the Bayer process [2]. The Hall–Héroult electrolytic process then transforms alumina into pure aluminium by dissolving it in molten cryolite and applying an electric current [2]. This deposits aluminium at the cathode while oxygen reacts with carbon anodes to produce carbon dioxide [3, 4]. Because the carbon anodes are consumed in this reaction, a continuous supply of high-quality anodes is critical for uninterrupted aluminium production.

Creating carbon anodes involves several key stages [5]. Initially, petroleum coke, coal tar pitch, and recycled anode materials are blended to form a uniform mix. This mix is then compacted into shape, often using vibro-compaction or molding techniques, resulting in green anodes. These green anodes undergo a baking process in specialized furnaces to enhance their structural, chemical, and thermal properties. Baking is essential as it increases the density and electrical conductivity of the anodes while reducing their reactivity with air. Once baked, the anodes go through the rodding phase, where they are equipped with attachments that allow them to be connected to the electrical circuit in the electrolytic cell.

The baking stage in anode production stands out as especially important due to its high energy consumption and its strong influence on the final quality of the anodes. Due to the complexity of the baking process, computational modelling, particularly using Computational Fluid Dynamics (CFD), is widely used to analyse and optimize furnace operations. In this regard, some investigations have focused on selecting the most suitable numerical models to simulate the key physical phenomena in the furnace. For example, the PDF (Probability Density Function) model is often recommended for combustion processes in heating section, the realizable k-ε model for turbulence, and the Discrete Ordinates Method (DOM) for radiative heat transfer [7]. Grégoire and Gosselin [6] performed a comparative study of three combustion models, Eddy-Dissipation, PDF, and a simplified combustion approach, highlighting how radiation significantly affects temperature profiles, while species diffusion influences flame behaviour slightly, and buoyancy plays a minor role in the firing section. Other studies have explored how to improve furnace efficiency and reduce energy use. Changes to the flue-wall geometry have led to better heat retention and more uniform baking of anodes. Designs that eliminate internal baffles have been shown to promote more even temperature distribution [8].

While CFD delivers detailed results, simplified models based on mass and energy balances offer a more practical and efficient alternative, for example for control purposes, enabling analysis of the entire furnace with significantly less computation time. Bui et al. [9] developed a one-dimensional model that includes both the flue and pit along the flow direction, though it does not account for flow redirection caused by internal baffles. Zhang et al. [10] later improved the model by representing the pit in two dimensions while keeping the flue channel one-dimensional. Further refinement was made in a subsequent study [11], where the flue channel was modelled in two dimensions to capture the effects of baffles, and the pit was simulated in a pseudo-3D format.

Based on the literature review, all CFD-based studies have concentrated on the heating section, with no research yet addressing the performance of the preheating section. Moreover, the existing simplified models are limited to cases without tie-bricks in the flue channel, making them less reliable for representing real furnaces used in smelters, where tie-bricks are commonly present. To address the gaps in previous studies, this work presents a CFD model of the preheating section of the anode baking furnace, along with an improved simplified model based on mass and energy conservation. The proposed simplified model accounts for the presence of tie-bricks in the flue channel, making it more representative of actual furnace configurations. Both models are then compared in terms of accuracy and computational cost.

2. System Overview

The anode baking process is carried out in an anode baking furnace, which consists of several connected sections with pits filled with green anodes and packed coke. A schematic of the anode baking furnace is depicted in Figure 1. The process is divided into three main zones: preheating, heating, and cooling, each playing a key role in determining the final anode quality. In the preheating zone, green anodes are gradually heated from room temperature to approximately 700–750 °C over a period of three to five days [6]. The slow temperature rise is essential to avoid internal cracks or structural failure. During this stage, volatile compounds from the pitch binder evaporate and diffuse through the porous anode and coke bed. These volatiles burn in the flue channels, providing about 40–50 % of the total furnace energy. To ensure safe and uniform heating, the rate is limited to around 15 °C per hour [11]. Once the anodes are preheated, they enter the heating zone, where the temperature is further raised to around 1 100 °C [6]. This is achieved using burners that supply the remaining 50–60 % of the total furnace energy. In this zone, carbonization of the pitch is completed, and the anodes reach their final baked structure. Proper temperature control in this phase is crucial to ensure uniform carbon quality and minimize defects. In the cooling zone, baked anodes gradually cool down to below 300 °C before being removed from the furnace [6]. Heat from the hot anodes is recovered and used to preheat

combustion air, which improves overall energy efficiency and reduces fuel consumption. Controlled cooling also prevents oxidation and thermal shock, ensuring the anodes are structurally intact and ready for the next stage, called rodding, where electrical connections are installed. The focus of this study is on the preheating section of the anode baking furnace.

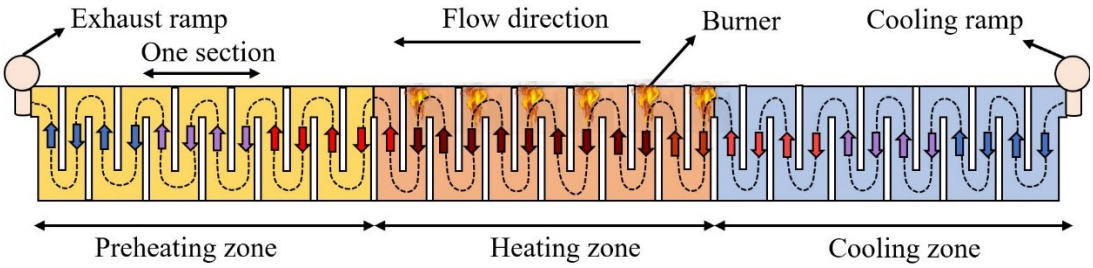

Figure 1. Schematic of the anode baking furnace.

3. Numerical Modelling

This study uses two distinct numerical methods to simulate the preheating section: a CFD model and a simplified approach based on mass and energy balance. Each method is presented individually in the sections that follow.

3.1 Computational Fluid Dynamics (CFD)

For the gas-phase simulation, the primary governing equations, namely the continuity, momentum, and energy equations, were employed. These equations are outlined below [6, 12]:

$$\frac{\partial \rho}{\partial t} + \nabla.\left(\rho \vec{V}\right) = 0 \tag{1}$$

$$\frac{\partial (\rho \vec{V})}{\partial t} + \nabla.\left(\rho \vec{V}\,\vec{V}\right) = -\nabla P + \nabla.\left((\mu + \mu_t)\left(\nabla \vec{V} + \nabla \vec{V}^T - \frac{2}{3}\nabla.\vec{V}\mathrm{I}\right)\right) - \frac{2}{3} I \nabla.(\rho k) + \rho \vec{g} \tag{2}$$

$$\frac{\partial (\rho h)}{\partial t} + \nabla.\left(\rho h \vec{V}\right) = \nabla.\left((k + \frac{\mu_t}{\mathrm{Pr}_t})\nabla T\right) + Q_{rad} \tag{3}$$

where:

ρ	Density, kg/m^3
$\vec{V}$	Velocity vector, m/s
P	Pressure, Pa
μ	Dynamic viscosity, Pa·s
μ_t	Turbulent dynamic viscosity, Pa·s
k	Thermal conductivity, W/m·K
$\vec{g}$	Gravitational acceleration vector, m/s^2
h	Specific enthalpy, J/kg
Pr_t	Turbulent Prandtl number
Q_{rad}	Radiative energy sources, W/m^3

As in the preheating section, when the anode temperature increases, volatiles including tar, methane, and hydrogen begin to be released. Due to the porous structure of the solid materials, these volatiles migrate into the flue channel, where they combust. To model the volatiles, the average anode temperature over time is tracked, and using Figure 3, the amount of each released volatile is calculated. It is then assumed that these volatiles enter the flue channel uniformly, where they undergo combustion. The combustion is modelled using the PDF approach based on

the mixture fraction method, requiring additional equations for mixture fraction and its variance [6, 12].

$$\frac{\partial \rho f}{\partial t} + \nabla.\left(\rho \vec{V} f\right) = \nabla.\left(\frac{\mu_t}{\sigma_t} \nabla f\right) \tag{5}$$

$$\frac{\partial (\rho f'^2)}{\partial t} + \nabla.\left(\rho \vec{V}\, \nabla f'^2\right) = \nabla.\left(\frac{\mu_t}{\sigma_t} \nabla f'^2\right) + C_g \mu_t (\nabla f'^2)^2 - C_d \rho \frac{\varepsilon}{k} f'^2 \tag{6}$$

where:

f Time-averaged mixture fraction

f'^2 Mixture fraction variance

Moreover, the empirical constants σ_t, C_g and C_d are set to 0.85, 2.86, and 2.0, respectively. The mixture fraction, f, is defined as follows:

$$f = \frac{Z_i - Z_{i,ox}}{Z_{i,fuel} - Z_{i,ox}} \tag{7}$$

where:

Z Mass fraction

Moreover, i, ox and fuel denote component i, oxidizer stream and fuel stream, respectively. In addition, the k-ε realizable model [13] is used for turbulence simulation, while the Discrete Ordinates Method (DOM) [14] models the thermal radiation in the flue channel.

In the solid domains, including the anodes, packing coke, and refractory bricks, only the heat conduction equation is solved, as given below:

$$\frac{\partial (\rho_s c_{ps} T_s)}{\partial t} = \nabla.\left(k_s \nabla T_s\right) \tag{4}$$

where:

T Temperature, K

c_p Heat capacity, J kg^{-1} K^{-1}

Moreover, s denotes the solid component.

3.2 Simplified Model

In this study, a pseudo-3D finite difference model was developed to simulate one section of the preheating zone. As shown in Figure 2, the presence of baffles divides each flue and pit into four regions, which are further split into control volumes. Energy equations are solved transiently for the solid, while mass, species, and energy balances for the gas phase assume a pseudo steady-state and are updated over time. The flue and pit are treated as separate sub-models, connected at the flue-side brick surface. To reduce computational cost, only half of the pit and flue is modelled by exploiting system symmetry.

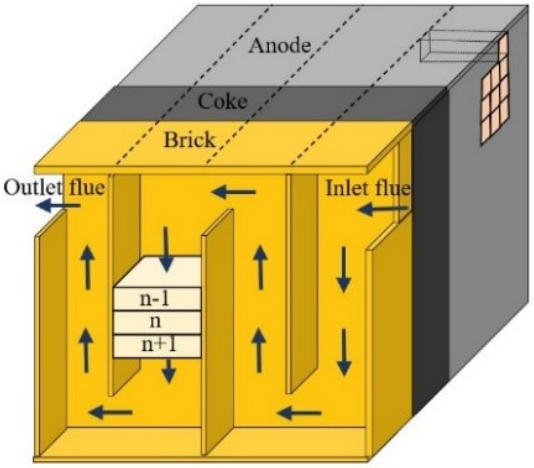

Figure 2. Schematic of the computational domain for a simplified model.

The pit sub-model evaluates transient heat conduction within the solid materials in two dimensions, as described by Equation (4). While, for each control volume in the flue, the thermal energy balance is calculated using the following equation [15]:

$$(Q_{gas\,inlet} - Q_{gas\,outlet}) + Q_{fuel} + Q_{volatiles} - (Q_{gas-solid} - Q_{solid-gas}) - (Q_{foundation} + Q_{atmosphere}) = 0 \quad (8)$$

The energy balance includes gas energy entering and exiting the control volume, heat released from fuel and volatile combustion, heat exchange between gas and solid, and heat losses to both the foundation and the atmosphere. The following provides a more in-depth description:

$$\dot{m}_g c_{pg}\left(T_{g.in} - T_{g.out}\right) + (\dot{m}_{tar}h_{tar} + \dot{m}_{H_2}h_{H_2} + \dot{m}_{CH_4}h_{CH_4}) - 2(h_c + h_r)DL\left(T_g - T_w\right) - LWh_{amb}\left(T_g - T_{amb}\right) = 0 \quad (9)$$

where:

$\dot{m}$	Mass flow rate, kg/s
D	Depth of the control volume, m
L	Length of the control volume, m
W	Width of the control volume, m

Moreover, g, in, out, tar, H_2 and CH_4, w and amb denote flue gas, inlet, outlet, tar volatile, H_2 volatile, CH_4 volatile, wall and ambient, respectively. h_c and h_r are calculated as follows [16]:

$$h_c = C\left(\frac{k_g}{D_h}\right)0.023\mathrm{Re}^{0.8}\mathrm{Pr}^{0.3} \quad (10)$$

$$h_r = \sigma\left(\frac{\varepsilon_g T_g^4 - \alpha_g T_w^4}{T_g - T_w}\right) \quad (11)$$

where:

D_h	hydraulic diameter, m
Re	Reynolds number
ε	Emissivity
α	Absorptivity

Moreover, C is a correction coefficient that accounts for the arrangement of tie-bricks within the channel. Volatile release from anode blocks strongly depends on anode temperature. Figure 3 presents the variation in the quantity of volatiles released throughout the baking process [9, 17].

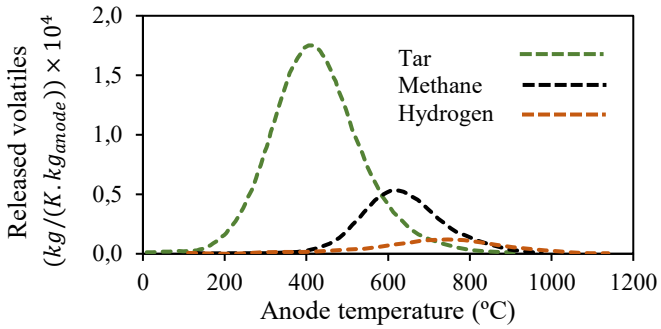

Figure 3. Instantaneous release rates of volatiles during the anode baking process [9, 17].

4. Validation

To validate the model, confidential data provided by Alcoa Corporation was used. The furnace under investigation is an open-top horizontal ring furnace. It consists of three preheating sections. Notably, the proposed models have the flexibility to evaluate different preheating designs across a wide range of dimensions and operating conditions. As such, the absence of confidential details does not affect its applicability or accuracy. The dataset includes flue gas temperature measurements at two locations within the preheating zone. Accordingly, the preheating section of the furnace was modelled using both numerical approaches described earlier, and the simulation results were compared with the measured values from the smelter. Due to confidentiality constraints, only dimensionless temperature values are presented. As shown in Figure 4, the simulated outlet air temperatures show strong agreement with the experimental data, demonstrating the accuracy of the models in representing the thermal behaviour of the preheating section. The maximum temperature deviation between the CFD model and the measured data is 7.3 °C, and for the simplified model, it is 5.2 °C. The corresponding average errors are 2.5 °C and 1.9 °C, respectively.

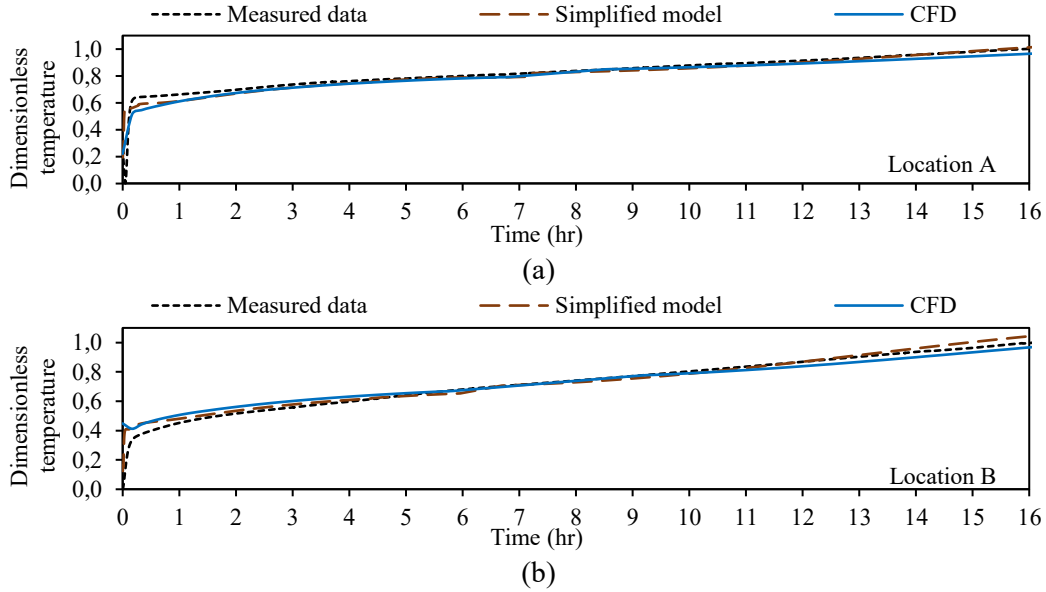

Figure 4. Comparison of predicted and measured flue gas temperatures at two different locations within the preheating section: (a) Location A and (b) Location B.

5. Results and Discussion

This section presents the results of the study. First, the preheating section is analyzed using a CFD approach. Then, a simplified model based on mass and energy conservation principles is applied to the same scenario. Finally, the results from both methods are compared. For this purpose, a hypothetical case is considered for the preheating process. The operational parameters in the present study are outlined as follows: The inlet air temperature is 1 000 °C, while the initial temperature of the solid is 700 °C. The air mass flow rate is 0.3 kg/s.

5.1 CFD Modelling

This section discusses the CFD modelling results for the preheating section. Figure 5 shows the airflow and velocity distribution in the preheating section. In this figure, in addition to the velocity contours and streamlines for the preheating section under study, which includes tie-bricks, a comparison case without tie-bricks is also presented. This allows for an assessment of the impact of the tie-bricks on the flow behavior. In the absence of tie-bricks, large vortices appear in certain parts of the flue channel, creating local recirculation zones. This causes air in other regions to speed up, leading to an uneven flow pattern. As a result, the heat transfer becomes unbalanced: faster-moving air loses less heat and stays warmer, while air caught in the vortices remains in the channel longer, losing more heat and reaching lower temperatures. The introduction of tie-bricks reduces the formation of large vortices, replacing them with smaller, localized eddies near the tie-bricks. This change leads to a more uniform flow pattern, lowers peak air velocities, and promotes smoother, more consistent airflow throughout the flue. This change in flow behavior leads to a more uniform heat transfer across the section.

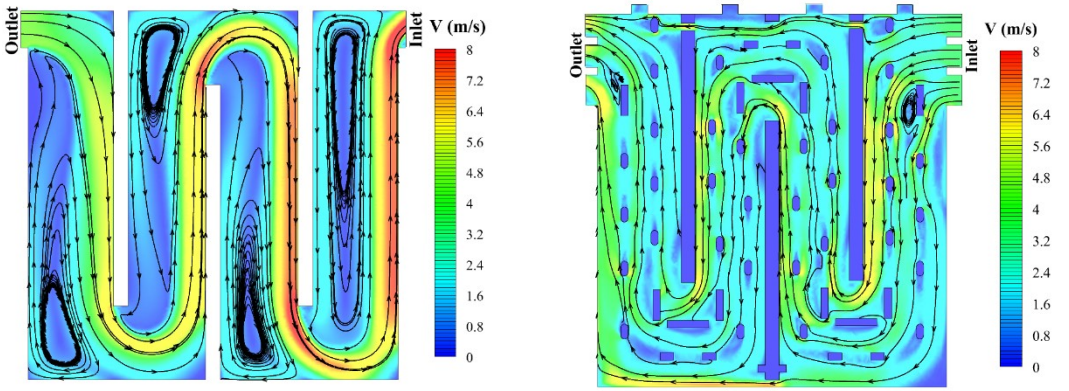

Figure 5. Velocity contours and streamlines are shown for (a) the configuration without tie-bricks and (b) the configuration with tie-bricks.

Figure 6 shows the temperature contours in the flue in the preheating section at two different time intervals: 5 hours and 17 hours after the start of the simulation. As shown, the flue gas temperature decreases as it flows through the preheating section, primarily due to heat transfer from the hotter flue gases to the cooler solid components. However, the preheating section is also affected by the release and combustion of volatile gases from the anodes. When these volatiles enter the flue channel and ignite, they temporarily increase the flue gas temperature, adding extra energy to the system. Despite this localized temperature rise from the combustion of volatiles, the overall trend is a gradual decline in flue gas temperature as it progresses through the channel, driven by continuous heat loss to the surrounding solid components. As the anode temperature increases over time, the heat transfer rate decreases due to the reduced temperature difference between the flue gases and the solid materials. This effect is evident when comparing the temperature profiles

at the two-time intervals, where the rate of temperature decrease becomes less noticeable over time as the system approaches thermal equilibrium.

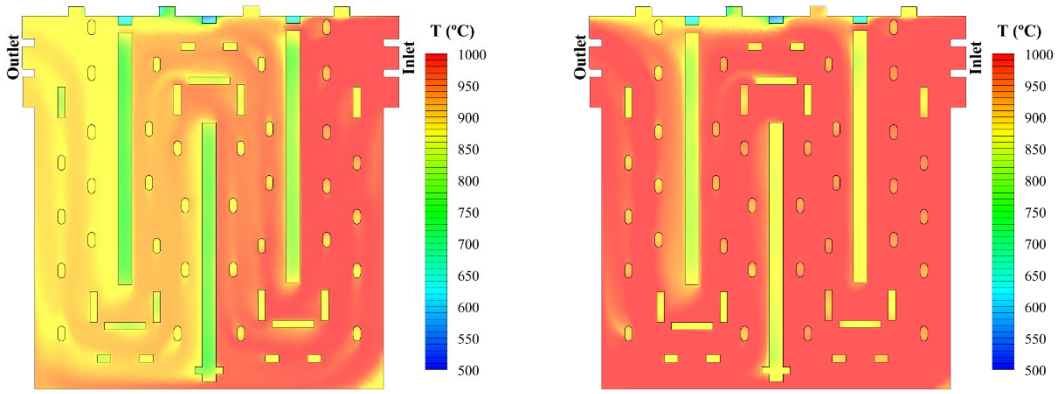

(a) (b)

Figure 6. Temperature contours in the preheating section: (a) 7 hours and (b) 15 hours after the start of the CFD simulation.

5.2 Simplified Modelling

This section presents the results from the modelling based on the principles of mass and energy conservation. The simplified model assumes that the flue velocity remains constant across any cross-section, which implies the absence of vortices or temperature imbalances along the flue path. As a result, the model cannot account for vortices or differentiate their sizes, making it unable to distinguish between the configuration with tie-bricks and the one without.

Therefore, to account for the presence of tie-bricks, the previous model must be modified by introducing a correction factor that reflects their impact on heat transfer, as shown in Equation (10). The correction factor is determined by comparing the results of the simplified model with the CFD outcomes for the configuration with tie-bricks. This factor varies based on the specific arrangement of the tie-bricks, as it depends solely on the tie-bricks arrangement. For the current arrangement, the correction coefficient is calculated to be 1.25. This value has been examined under various operating conditions, including cooling, heating and preheating zones, and the results consistently indicate the same value for this tie-brick arrangement. Therefore, it can be confidently stated that this coefficient is accurate and depends solely on the tie-bricks arrangement.

Figure 7 shows the temperature distribution in the preheating section. As depicted, the flue temperature gradually decreases as it loses heat to the surrounding solid materials. However, it is important to note that the introduction of volatiles into the flue channel, followed by their combustion, temporarily raises the flue temperature by injecting additional energy into the system. Despite this temporary increase, after 7 hours of system operation, the anode temperature has not risen significantly. As a result, the amount of volatiles released and the energy generated from their combustion have not been substantial. Therefore, the overall trend remains a gradual decrease in flue temperature as it moves through the channel, primarily due to significant heat loss from the flue gases to the anodes. However, over time, it is observed that after 15 hours of system operation, the rate of temperature increase at the anodes accelerates. The release of volatiles and the energy generated from their combustion begin to have a more pronounced effect on the air temperature inside the channel, causing localized increases in air temperature in certain areas.

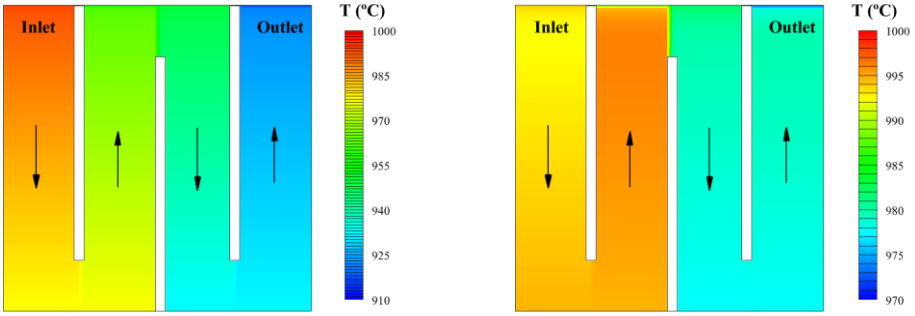

(a) (b)

Figure 7. Temperature contours in the flue (a) 7 hours and (b) 15 hours after the start of the simplified modelling.

5.3 Comparison of Numerical Models

The primary objective of this research is to evaluate the accuracy of the simplified numerical model, based on the principles of mass and energy conservation, by comparing it with the results from CFD modelling. This section presents a comparison of the results obtained from the simplified model with those from the CFD model. The parameters compared include the temperatures of the anode, coke, refractory bricks, and outlet air. The comparison is illustrated in Figure 8. There is an average temperature prediction discrepancy of 5 ºC between the CFD model and the simplified model based on mass-energy conservation. Moreover, while the CFD simulation requires approximately three hours of computational time per furnace section, the simplified model achieves equivalent precision in just three seconds, providing an unparalleled combination of speed and reliability.

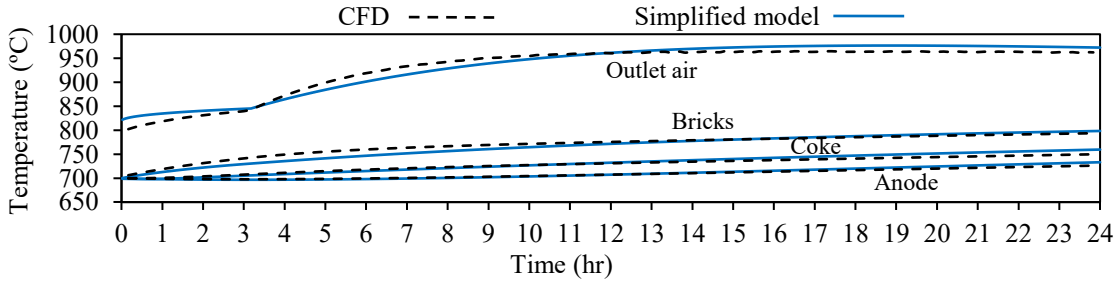

Figure 8. Comparison of temperature profiles between CFD and simplified models.

Therefore, the simplified model is well-suited for routine operations, monitoring, and assessments where quick results and low computational costs are beneficial. In contrast, CFD simulations are essential in more complex scenarios, such as design optimization, failure analysis, or modifications to geometry and boundary conditions, where high spatial resolution and greater accuracy are required.

6. Conclusions

Anode baking is one of the most critical phases in the anode production process, as it directly impacts the quality of the anodes and is the most-costly and energy-intensive step. One of the most important zones within this process is the preheating zone. In this study, two approaches are developed to analyse the preheating process: one based on Computational Fluid Dynamics (CFD), and the other an improved version of previous models based on the mass and energy conservation principles, which have been refined and enhanced through this research. These models are then

evaluated and compared in terms of accuracy and computational efficiency. The key contributions of this research are as follows:

- Our findings show a maximum temperature prediction discrepancy of just 1.5 % between the CFD model and the modified simplified model based on mass-energy conservation.
- Furthermore, while the CFD simulation requires approximately three hours of computational time per furnace section, the simplified model achieves equivalent precision in just three seconds, significantly reducing both computational time and associated financial costs, offering an unprecedented combination of speed, reliability, and affordability.

7. Acknowledgements

The authors are grateful to the Natural Sciences and Engineering Research Council of Canada (NSERC) and to Alcoa for their financial supports. Moreover, part of the research presented in this work was financed by the Fonds de recherche du Québec – Nature et technologies, through the Aluminium Research Centre – REGAL.

8. References

1. P. Ponnusamy, R.A. Rahman Rashid, S.H. Masood, D. Ruan, S. Palanisamy. Mechanical properties of SLM-printed aluminium alloys: a review. *Materials*. 13 (2020) 4301.
2. R. Zhao, C. Nowicki, L. Gosselin, C. Duchesne. Energy and exergy inventory in aluminium smelter from a thermal integration point-of-view. *International Journal of Energy Research*. 40 (2016) 1321-1338.
3. Q. Wang, L. Gosselin, M. Fafard, J. Peng, B. Li. Numerical investigation on the impact of anode change on heat transfer and fluid flow in aluminium smelting cells. *Metallurgical and Materials Transactions B. 47* (2016) 1228-1236.
4. O. Lassagne, L. Gosselin, M. Désilets, M.C. Iliuta. Techno-economic study of CO2 capture for aluminium primary production for different electrolytic cell ventilation rates. *Chemical Engineering Journal*. 230 (2013) 338-350.
5. S. Zheng, Z. Rao, S. Liao. Structural and thermal analysis of an innovative baking furnace for carbon anode production. *International Journal of Energy Research*. 45 (2021) 6907-6921.
6. F. Grégoire, L. Gosselin. Comparison of three combustion models for simulating anode baking furnaces. *International Journal of Thermal Sciences*. 129 (2018) 532-544.
7. A.R. Tajik, T. Shamim, M. Zaidani, R.K.A. Al-Rub. The effects of flue-wall design modifications on combustion and flow characteristics of an aluminium anode baking furnace-CFD modeling. *Applied Energy*. 230 (2018) 207-219.
8. Y.E. Ghaoui, S. Besson, Y. Drouet, F. Morales, A. Tomsett, M. Gendre, et al. Anode baking furnace fluewall design evolution: a return of experience of latest baffleless technology implementation. *Light Metals 2016*. (2016) 941-945.
9. R.T. Bui, A. Chartette, T. Bourgeois. A computer model for the horizontal flue ring furnace. *IEEE transactions on industry applications*. (1984) 894-901.
10. L. Zhang, C. Zheng, M. Xu. Simulating the heat transfer process of horizontal anode baking furnace. *Developments in Chemical Engineering and Mineral Processing*. 13 (2005) 447-458.
11. N. Oumarou, D. Kocaefe, Y. Kocaefe. An advanced dynamic process model for industrial horizontal anode baking furnace. *Applied Mathematical Modelling*. 53 (2018) 384-399.
12. ANSYS fluent theory guide, release 14.5, ANSYS Inc, 2012.
13. K. Saqr, M. Wahid. Comparison of four eddy-viscosity turbulence models in the eddy dissipation modeling of turbulent diffusion flames. *International Journal of Applied Mathematics and Mechanics*. 7 (2011) 1-18.

14. G. Colomer, M. Costa, R. Consul, A. Oliva. Three-dimensional numerical simulation of convection and radiation in a differentially heated cavity using the discrete ordinates method. *International Journal of Heat and Mass Transfer*. 47 (2004) 257-269.
15. M. Zaidani, A.R. Tajik, Z.A. Qureshi, T. Shamim, R.K.A. Al-Rub. Investigating the flue-wall deformation effects on performance characteristics of an open-top aluminium anode baking furnace. *Applied Energy*. 231 (2018) 1033-1049.
16. F.P. Incropera, D.P. DeWitt, T.L. Bergman, A.S. Lavine. Fundamentals of heat and mass transfer. *Wiley New York 1996*.
17. E. Dernedde, A. Charette, T. Bourgeois, L. Castonguay. Kinetic phenomena of the volatiles in ring furnaces. *Light Metals* 1986. 589-592.